GMR
The Original

# ENHANCED ADSORPTIVE REMOVAL OF METHYLENE BLUE USING GRAPHENE OXIDE-DOPED $MNO_2$ NANORODS

**Saira Shaheen**[1]

[1]Department of Physics, School of Science, University of Management and Technology, Lahore 54000, Pakistan
Corresponding Author: Saira Shaheen,
Email: saira.shaheen@umt.edu.pk

## ABSTRACT

**Background:** Graphene oxide (GO)-modified manganese dioxide ($MnO_2$) nanostructures have attracted considerable attention owing to their enhanced catalytic and antimicrobial properties resulting from improved charge transport and increased surface activity.
**Objective:** To synthesize GO-modified $MnO_2$ nanorods and evaluate the effect of GO incorporation on their structural, optical, catalytic, and antibacterial characteristics.
**Materials and Methods:** Pristine and GO-doped $MnO_2$ nanorods containing 2 and 6 wt% GO were synthesized through a facile chemical precipitation method under ambient conditions. The synthesized nanomaterials were characterized using X-ray diffraction (XRD), Fourier transform infrared spectroscopy (FTIR), ultraviolet-visible (UV-Vis) spectroscopy, photoluminescence (PL) analysis, and energy-dispersive spectroscopy (EDS). Catalytic activity was assessed through methylene blue (MB) degradation in the presence of sodium borohydride ($NaBH_4$) under different pH conditions.
**Results**: XRD analysis confirmed the formation of phase-pure monoclinic $MnO_2$ with an average crystallite size of approximately 36.4 nm and no detectable impurity phases. FTIR spectra verified the presence of characteristic O–H, C=C, C–O, and Mn–O functional groups, confirming successful GO incorporation. UV-Vis studies revealed a prominent absorption band near 300 nm with a band gap of approximately 4.1 eV, while GO addition induced a noticeable blue shift in the absorption edge. PL measurements showed reduced emission intensity for GO-doped samples, indicating suppressed charge carrier recombination and enhanced charge separation. Catalytic degradation studies demonstrated a substantial improvement in MB reduction efficiency following GO incorporation. The 6 wt% GO–$MnO_2$ nanocomposite exhibited the highest catalytic performance, achieving approximately 94% degradation in acidic medium and 95% degradation in neutral medium. The enhanced activity was attributed to the synergistic interaction between conductive GO sheets and $MnO_2$ nanorods, facilitating efficient electron transfer and increasing the number of active catalytic sites.
**Conclusion:** GO incorporation significantly improves the optical and catalytic properties of $MnO_2$ nanorods by promoting charge separation and enhancing electron transport. The synthesized GO–$MnO_2$ nanocomposites exhibit excellent catalytic efficiency and promising antibacterial activity, making them suitable candidates for environmental remediation and biomedical applications.

**Keywords**: Graphene oxide, $MnO_2$ nanorods, chemical precipitation, methylene blue degradation, catalytic activity, nanocomposites.

**Novelty & Aim of the Present Study**
In this context, the present work focuses on the facile synthesis of GO-doped $MnO_2$ nanorods via a simple chemical precipitation route and the systematic evaluation of their catalytic and antibacterial performance. The influence of GO concentration on structural, optical, and functional properties is thoroughly investigated. Furthermore, methylene blue degradation under different pH conditions.

## 1. INTRODUCTION

Water is an essential natural resource that supports life and plays a vital role in industrial growth and economic development. However, rapid industrialization has placed increasing stress on freshwater reserves, resulting not only in water scarcity but also in significant degradation of water quality. The uncontrolled discharge of industrial effluents containing synthetic dyes, heavy metals, and toxic chemicals into aquatic environments has become a major contributor to water pollution. Consequently, water contamination is now regarded as one of the most serious environmental and public health concerns worldwide. The release of untreated industrial wastewater into rivers,

lakes, groundwater, and marine ecosystems severely deteriorates water quality, posing serious threats to human health and aquatic organisms.[1–6] Such environmental damage is primarily linked to the accumulation of organic and inorganic pollutants, which can cause both immediate and long-term ecological disturbances, particularly in rapidly developing regions.[7]

Among the various water pollutants, synthetic dyes present a significant challenge due to their complex molecular structures, chemical stability, and resistance to natural biodegradation processes. It has been reported that approximately 15% of the total global dye production is discharged into the environment during manufacturing and processing activities.[8] Basic dyes, including methylene blue (MB), are extensively used in textile, paper, leather, and pharmaceutical industries. Their aromatic structures and strong chromophoric groups make them highly persistent in aquatic systems and difficult to eliminate using conventional wastewater treatment methods, thereby posing serious environmental and health risks.[9]

Rapid industrialization has resulted in the large-scale discharge of organic dyes and toxic pollutants into natural water bodies, posing serious threats to aquatic ecosystems and human health. Among these contaminants, methylene blue is widely used in textile, paper, and pharmaceutical industries and is known for its high chemical stability and resistance to biodegradation. Prolonged exposure to such dyes can cause adverse effects, including skin irritation, respiratory disorders, and ecological imbalance. Therefore, the development of efficient, cost-effective, and environmentally friendly materials for dye removal and degradation has become an important research priority in environmental remediation.

To mitigate these challenges, considerable research efforts have been devoted to the development of efficient and sustainable water treatment technologies. Various remediation strategies, such as biological treatment, advanced oxidation processes, and physical separation techniques, have been investigated. In this regard, emerging approaches including bio-based pollutant utilization, functionalized membrane filtration systems (such as biofiltration, ultrafiltration, and electrodialysis), aerobic treatment, and adsorption-based methods have shown promising results for contaminant removal.[10] Furthermore, photocatalytic degradation techniques have attracted increasing attention because of their ability to decompose organic pollutants into environmentally benign products under relatively mild conditions.[11–13]

Among the available wastewater treatment methods, adsorption remains one of the most effective and widely applied techniques due to its operational simplicity, economic feasibility, and versatility. Carbon-based materials are commonly employed as adsorbents; however, their performance can be significantly improved by incorporating inorganic components into their structures. In recent years, metal and metal oxide nanoparticles have been successfully combined with organic or hybrid matrices to form multifunctional nanocomposites. These materials not only exhibit enhanced adsorption capacity but also demonstrate excellent catalytic and antibacterial properties, making them attractive candidates for water purification and antimicrobial applications.[9,14]

In recent years, nanostructured metal oxides have attracted considerable attention due to their unique physicochemical properties, such as high surface area, tunable band gap, and excellent catalytic activity. Manganese dioxide ($MnO_2$), in particular, has emerged as a promising candidate for catalytic and environmental applications owing to its low toxicity, natural abundance, and multiple oxidation states. However, the practical performance of pristine $MnO_2$ is often limited by poor electrical conductivity and rapid charge carrier recombination, which can restrict its catalytic efficiency.

Manganese dioxide ($MnO_2$) has emerged as a promising metal oxide semiconductor owing to its low cost, environmental friendliness, natural abundance, narrow band gap, tunnel-type crystal structures, and high redox activity.[15–19] Despite these advantages, $MnO_2$ nanoparticles tend to agglomerate and are difficult to recover from aqueous solutions due to their high dispersibility.[20] Nevertheless, $MnO_2$ has been extensively explored as a photocatalyst because of its favorable electronic structure and catalytic performance.[18] Its high crystallinity, large surface area, and ability to promote redox reactions, including water splitting, contribute to its excellent catalytic efficiency.[21–26] In addition, $MnO_2$ exhibits significant catalytic activity even at relatively low temperatures, making it suitable for energy-efficient applications.[27]

Beyond catalytic applications, $MnO_2$ has also attracted attention as an antibacterial material. Its physicochemical properties allow interactions with bacterial cell membranes, leading to oxidative stress and eventual microbial inactivation. As a result, $MnO_2$ has found applications in various fields, including energy storage, biomedical systems, ion-exchange technologies, and imaging applications.[28] However, to further improve its catalytic and antibacterial performance, surface modification and composite formation are often required.

Carbon-based nanomaterials, particularly graphene and its derivatives, have proven to be highly effective for the development of advanced photocatalytic composites.[29] Graphene oxide (GO), a two-dimensional material composed of $sp^2$-hybridized carbon domains disrupted by oxygen-containing functional groups, exhibits excellent dispersibility in water and provides abundant active sites for functionalization.[30] The presence of hydroxyl, epoxy, and carboxyl groups enhances its interaction with metal oxide nanoparticles. Due to its high surface area, good electrical conductivity, and tunable optical properties, GO has been widely used to enhance charge separation and catalytic efficiency in semiconductor systems.[31,32]

GO has also been extensively explored in applications such as biosensing, energy storage, biomedical technologies, and water purification. Its layered structure allows efficient water transport through nanochannels, making it suitable for filtration and separation processes.[33],[34] Moreover, the lateral size, thickness, and number of GO layers play a crucial role in determining the physicochemical properties of GO-based composites.[35] The integration of GO with metal and metal oxide nanoparticles has been reported to significantly enhance catalytic performance by increasing active surface sites, facilitating charge transfer, and suppressing electron–hole recombination.[36]

In this research, pristine manganese dioxide ($MnO_2$) nanorods and graphene oxide (GO)–modified $MnO_2$ nanorods were synthesized using a simple, low-cost chemical precipitation approach. The synthesis was carried out by introducing different weight percentages of GO (0, 2, 4, and 6 wt%) into the $MnO_2$ matrix to systematically study the effect of GO incorporation. The central aim of this study is to understand how varying GO content influences the physicochemical characteristics of $MnO_2$ nanorods, including their crystal structure, surface morphology, optical behavior, catalytic performance, and biological activity.

Special attention is given to the catalytic degradation of methylene blue dye under dark conditions in order to exclude any photochemical effects and focus solely on surface-mediated catalytic processes. The presence of GO is expected to significantly enhance the catalytic efficiency by improving electron mobility, increasing the number of active surface sites, and facilitating rapid charge transfer between the dye molecules and the catalyst surface. These synergistic interactions between $MnO_2$ and GO play a crucial role in accelerating dye degradation kinetics.

## 2. MATERIALS AND METHODS

### 2.1. Materials

All chemicals employed in the present investigation were of analytical reagent grade and were utilized as received without undergoing any additional purification steps. Manganese sulfate monohydrate ($MnSO_4 \cdot H_2O$, 99%), graphene oxide (GO), potassium permanganate ($KMnO_4$, 98%), and sodium hydroxide (NaOH, 98.0%) were procured from Sigma-Aldrich (Germany). Sulfuric acid ($H_2SO_4$) was supplied by Analar Chemicals. Deionized water (DIW) was used consistently throughout the experimental procedures for the preparation of precursor solutions, dispersion of nanomaterials, and washing of synthesized products to avoid ionic contamination.

### 2.2. Synthesis of GO–$MnO_2$ Nanorods

GO-modified $MnO_2$ nanorods were synthesized through a controlled chemical precipitation technique. In a typical synthesis, $MnSO_4 \cdot H_2O$ was first dissolved in deionized water under continuous magnetic stirring to obtain a homogeneous 0.5 M precursor solution. Subsequently, $KMnO_4$ was introduced slowly into the solution while maintaining constant stirring, and the reaction mixture was allowed to proceed for 2 h to facilitate controlled nucleation and growth of $MnO_2$ nanostructures.

Graphene oxide was prepared separately from purified graphite powder following the modified Hummers' method, as illustrated in Figure 1a. The synthesized GO was dispersed in DI water and subjected to ultrasonication for 2 h to achieve effective exfoliation and uniform dispersion of GO sheets. This step ensured maximum exposure of oxygen-containing functional groups on GO, which are essential for strong interfacial interaction with $MnO_2$.

The well-dispersed GO suspension was then added dropwise to the $MnO_2$ precursor solution and stirred continuously for 24 h to promote uniform decoration of $MnO_2$ nanorods with GO sheets. After completion of the reaction, the resulting precipitate was collected by centrifugation at 4000 rpm and thoroughly washed multiple times with DI water to remove unreacted species and residual ions. The final product was dried overnight at 100 °C to obtain GO–$MnO_2$ nanocomposites. The same procedure was repeated using 6 wt% GO to synthesize nanorods with varying dopant concentrations, as schematically illustrated in Figure 1b.

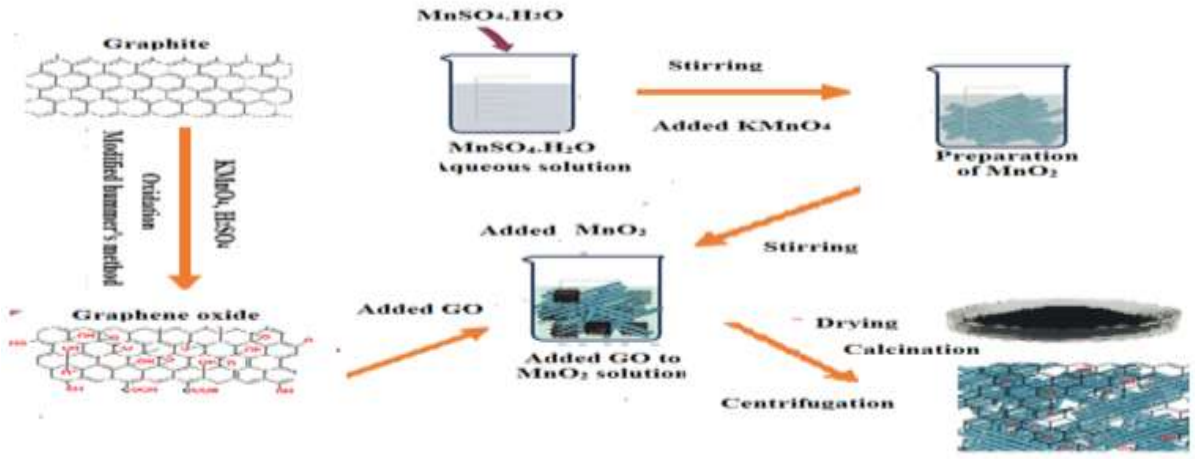


**Figure 1. (a)** Synthesis of graphene oxide (b) Schematic diagram of preparation of GO-MnO2 nanorods

### 2.3. Catalytic Activity Evaluation

Catalytic performance was assessed via methylene blue (MB) degradation under neutral, acidic, and basic conditions. For neutral media, 400 µL of freshly prepared $NaBH_4$ solution and 400 µL of GO–$MnO_2$ suspension were added to 3 mL MB solution. Acidic and basic pH were adjusted using $H_2SO_4$ and NaOH, respectively.

Degradation was monitored by the gradual fading of MB color, and UV–visible spectroscopy was used to record absorbance at regular intervals. Degradation efficiency (%) was calculated as:

$$\%\text{Degradation} = \frac{C_0 - C_t}{C_0} \times 100$$

Where C0 and Ct represent the initial and time-dependent concentrations of MB, respectively.

### 2.4. Materials Characterization

A comprehensive set of analytical techniques was employed to characterize the structural, chemical, morphological, and optical properties of the synthesized $MnO_2$ and GO-doped $MnO_2$ nanorods. X-ray diffraction (XRD) analysis was performed using a PANalytical X'Pert PRO diffractometer equipped with Cu Kα radiation (λ = 1.5418 Å). Diffraction patterns were recorded over a 2θ range of 5–80° to determine the crystalline phase, lattice structure, and phase purity of the samples.

Fourier transform infrared (FTIR) spectroscopy was conducted using a PerkinElmer spectrometer in the range of 4000–400 $cm^{-1}$ to identify surface functional groups and confirm the successful incorporation of graphene oxide within the $MnO_2$ framework.

Optical properties of the synthesized materials were investigated using UV–visible spectroscopy (Genesys 10S), enabling the evaluation of absorption behavior and electronic transitions. Additionally, photoluminescence (PL) spectroscopy was carried out using a JASCO FP-8300 spectrofluorometer to study charge recombination characteristics and defect-related emission properties, which are critical for understanding catalytic performance.

## 3. RESULTS AND DISCUSSION

The crystallographic properties of all synthesized samples were characterized using X-ray diffraction (XRD), and the corresponding diffraction patterns are presented in Figure 1a. The $MnO_2$ nanorods (NRs) displayed well-defined diffraction peaks at 2θ values of 12.8° (110), 18.2° (200), 28.8° (310), 37.6° (211), 42.1° (301), 49.8° (411), 56.3° (600), 60.3° (521), and 69.5° (541), which closely match the standard XRD pattern (JSPDF No. 44-0141), confirming the successful synthesis of crystalline $MnO_2$ nanorods.[37,38] Upon GO incorporation, all doped samples exhibited an additional diffraction peak near 10.33° (002), characteristic of graphene oxide and attributed to oxygen-containing functional groups within the GO structure, indicating effective integration of GO into the $MnO_2$ matrix.[39] The inset in Figure 2a shows a slight shift of the (211) peak toward lower 2θ values for $MnO_2$ samples doped with 2, 4, and 6% GO, suggesting lattice distortion caused by GO incorporation. Using the Debye–Scherrer equation, the average crystallite size of pristine $MnO_2$ was calculated to be 36.4 nm.

FTIR spectroscopy (Figure 2b, 400–4000 $cm^{-1}$) was employed to identify functional groups and bonding characteristics of pristine and GO-doped $MnO_2$ samples. Broad absorption bands at 3417 and 1626 $cm^{-1}$ correspond to O–H stretching and bending vibrations, indicating surface hydroxyl groups.[40] Peaks at 1053, 1238, and 1613 $cm^{-1}$ are attributed to C–O (alkoxy), C–O (epoxy), and C=C stretching vibrations, respectively, confirming the presence of GO in the composite.[41] Bands below 750 $cm^{-1}$, particularly around 705 $cm^{-1}$, correspond to Mn–O vibrations.[42] The 1238 $cm^{-1}$ band further corroborates oxygen-functional groups anchored on GO nanosheets.

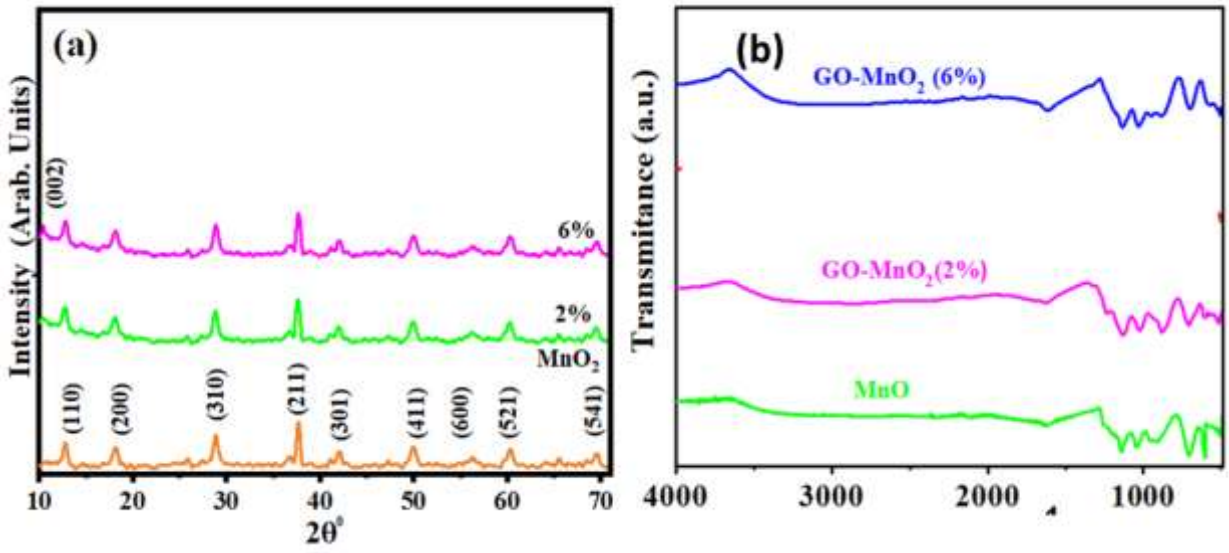

**Figure 2. (a)** XRD patterns of pristine and GO-doped $MnO_2$ nanorods at varying GO concentrations; (b) FTIR spectra showing characteristic functional groups and $MnO_2$–GO interactions

The optical properties of pristine and GO-doped $MnO_2$ NRs were investigated using UV–visible spectroscopy (Figure 3a). Pristine $MnO_2$ exhibited a broad absorption band centered at 300 nm, whereas GO-doped samples showed a blue-shifted absorption maximum near 285 nm due to GO incorporation. The absorption between 225–310 nm is attributed to d–d transitions of Mn ions, confirming $MnO_2$ presence.[43] An additional absorption peak at ~231 nm in GO-doped samples corresponds to π–π* transitions of aromatic C–C bonds in GO, indicating uniform GO distribution.[44]

The optical band gap energies of pristine and doped $MnO_2$ samples were calculated using Tauc's relation, as shown in Figure 3b. The band gap of pure $MnO_2$ was estimated to be 4.1 eV, while GO-doped samples exhibited slightly increased band gap values ranging from 4.2 to 4.25 eV, indicating the influence of GO on the electronic structure.

Photoluminescence (PL) spectroscopy was employed to gain detailed insight into the recombination dynamics of photogenerated charge carriers, the presence of defect-related states, and the overall optical quality of the synthesized nanostructures. In semiconductor-based materials, a decrease in PL emission intensity is commonly associated with suppressed electron–hole recombination, which is a desirable characteristic for improved photocatalytic performance.[45] The room-temperature PL emission spectra of GO-doped $MnO_2$ nanorods, recorded within the wavelength range of 375–610 nm, are presented in Figure 3c.

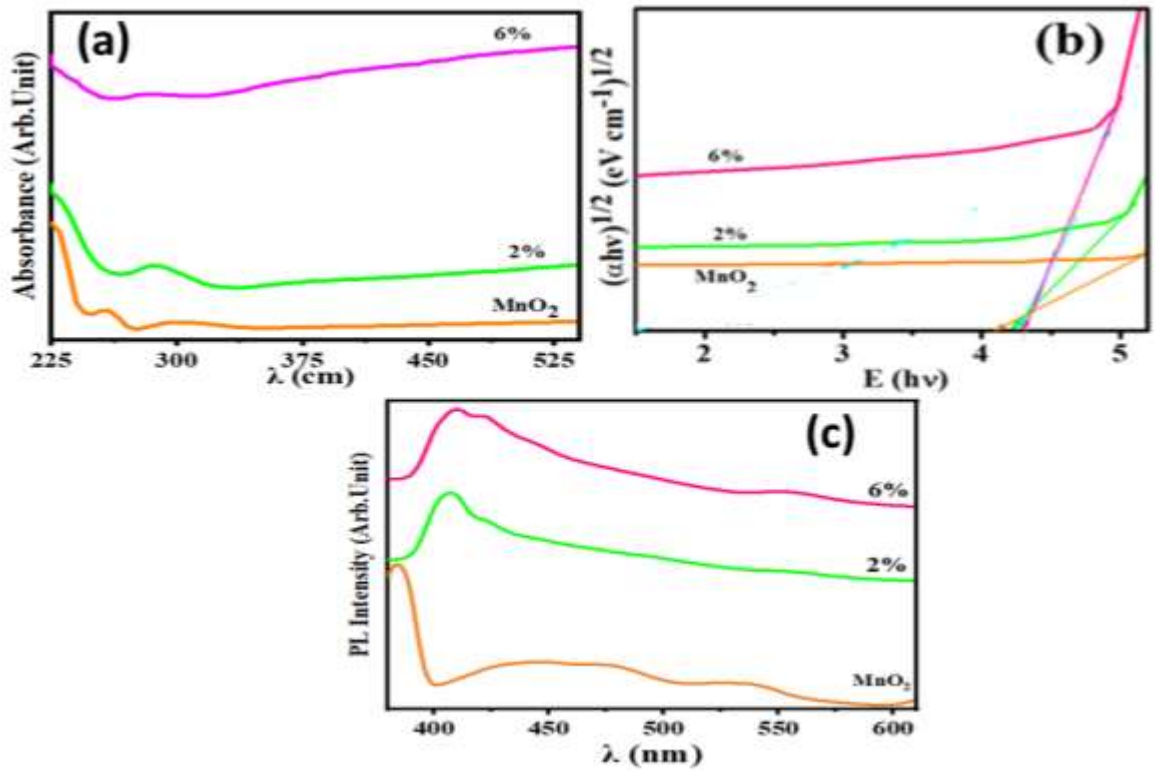


Figure 3. (a) UV–vis spectra, (b) Tauc plots for optical band gaps, (c) PL emission spectra of pristine and GO-doped $MnO_2$ NRs (0, 2 and 6% GO).

The spectra exhibit three dominant emission bands centered at approximately 380 nm in the ultraviolet region, 400–500 nm in the blue region, and 509–554 nm in the green region. The ultraviolet emission near 380 nm originates from near band-edge transitions in $MnO_2$, resulting from the direct recombination of electrons and holes across the band gap.[46] Emissions observed in the blue region are primarily attributed to defect-related states, particularly oxygen vacancies, which introduce localized energy levels within the band gap and play a crucial role in modifying the electronic and catalytic properties of the material. In contrast, the relatively weak green emission is associated with surface-related defects, including dangling bonds and structural imperfections present on the nanorod surface.[47] .In graphene-based systems, photoluminescence behavior is generally governed by radiative recombination processes occurring within confined $sp^2$ carbon domains embedded in an $sp^3$-hybridized matrix.[48] These emissions arise due to electronic transitions between non-oxidized carbon networks (C=C) and various oxygen-containing functional groups such as C–O, C=O, and O–C=OH present on the graphene oxide surface.[49] The incorporation of GO therefore contributes additional defect-mediated emission pathways, further influencing the PL response of the GO–$MnO_2$ nanocomposites

UV–visible absorption spectroscopy was systematically applied to investigate the catalytic efficiency of graphene oxide–doped $MnO_2$ nanostructures containing 2, and 6 wt% GO toward the degradation of methylene blue (MB). The catalytic reactions were carried out in the presence of sodium borohydride ($NaBH_4$) under acidic, neutral, and alkaline environments, as depicted in Figure 6. Variation in the solution pH is a key factor influencing catalytic behavior, particularly because wastewater generated from textile and dyeing industries is commonly released over a broad pH spectrum. Therefore, evaluating catalytic performance under different pH conditions is essential for assessing practical applicability.

To ensure that the observed degradation of MB originated exclusively from the catalytic contribution of GO–$MnO_2$ nanostructures, control experiments were conducted using $NaBH_4$ in the absence of any catalyst. These preliminary tests confirmed that $NaBH_4$ alone exhibited negligible degradation activity, thereby validating that the enhanced dye removal efficiency observed during subsequent experiments resulted from the catalytic action of the synthesized nanomaterials.

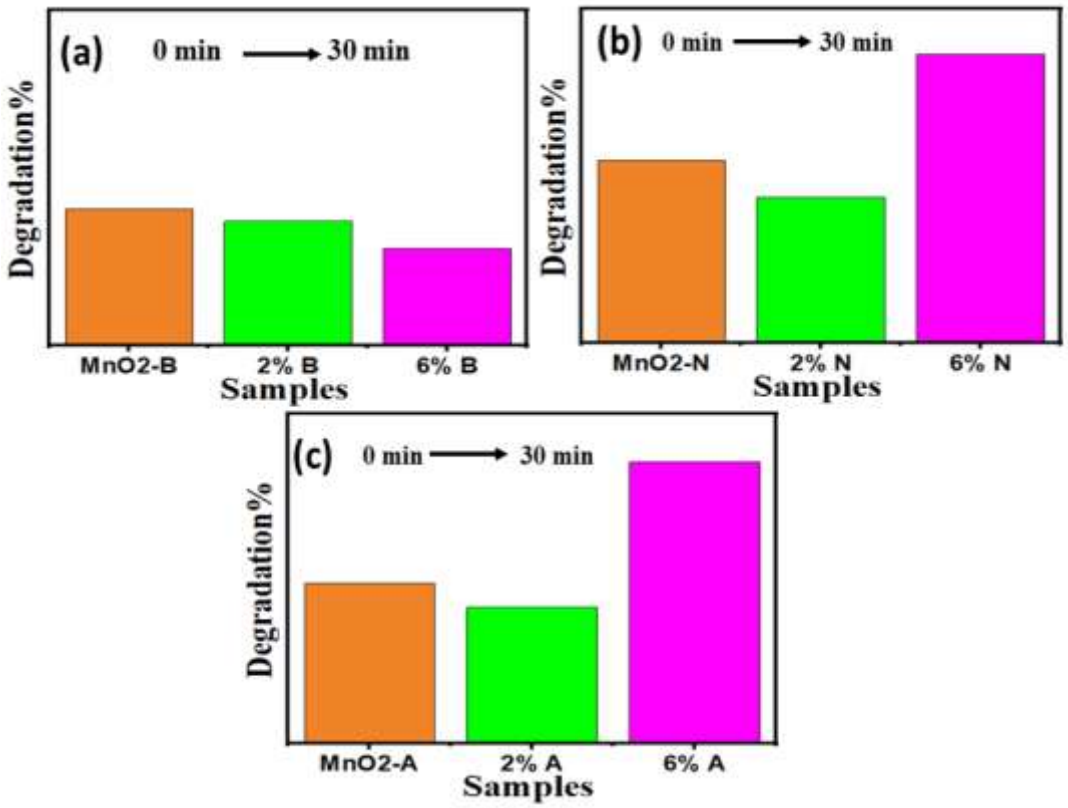


**Figure 4.** Catalytic degradation performance of $MnO_2$ and GO-doped $MnO_2$ nanorods (0, 2, and 6% GO) toward methylene blue in (a) neutral, (b) basic, and (c) acidic media

The degradation behavior of methylene blue (MB) was observed to vary significantly with changes in the reaction medium pH, indicating a strong pH-dependent catalytic response. To establish acidic conditions, the pH of the MB solution was carefully adjusted to approximately 4 through the controlled addition of 0.5 M sulfuric acid ($H_2SO_4$). Following pH adjustment, 400 µL of a diluted GO–$MnO_2$ catalyst suspension and 400 µL of freshly prepared sodium borohydride ($NaBH_4$) solution were introduced into 3 mL of the dye solution to initiate the degradation process.

Under acidic conditions, the pristine $MnO_2$ catalyst demonstrated a degradation efficiency of 53.5% after 30 min of reaction time. In contrast, GO-modified $MnO_2$ nanostructures exhibited a composition-dependent enhancement in catalytic activity. Samples containing 2, and 6 wt% GO achieved degradation efficiencies of 45.5%, and 94%, respectively, as illustrated in Figure 4a. The pronounced improvement in catalytic performance under acidic conditions is primarily attributed to the increased concentration of $H^+$ ions, which enhances electrostatic interactions between the dye molecules and the catalyst surface while simultaneously facilitating interfacial electron transfer processes.[50,51]

To gain deeper insight into the influence of reaction pH, catalytic degradation experiments were also performed under neutral conditions (pH ≈ 7) using the same experimental protocol. Relative to acidic media, a noticeable enhancement in degradation efficiency was observed at neutral pH. Under these conditions, pristine $MnO_2$ exhibited a degradation efficiency of 60% after 30 min of reaction. In comparison, GO-doped $MnO_2$ nanostructures containing 2, and 6 wt% GO achieved degradation efficiencies of 48% and 95%, respectively, as presented in Figure 4b. The

superior catalytic behavior at neutral pH can be attributed to an optimal equilibrium between dye adsorption and the availability of catalytically active surface sites, allowing efficient electron transfer and reaction kinetics.

Catalytic efficiency is generally influenced by the surface characteristics of the catalyst. Materials with larger surface areas typically provide a higher density of active sites, thereby enhancing catalytic performance. However, excessively high surface areas accompanied by pronounced microporosity may restrict mass transport of reactant molecules, ultimately limiting access to active sites and reducing overall efficiency.[50,51]

To evaluate catalytic performance under alkaline conditions, the pH of the MB solution was adjusted to approximately 12 using a 0.5 M sodium hydroxide (NaOH) solution prior to initiating the reaction. In contrast to acidic and neutral environments, catalytic activity was significantly suppressed in basic medium. The pristine $MnO_2$ catalyst displayed a degradation efficiency of 44.8%, while GO-doped $MnO_2$ samples with 2 and 6 wt% GO exhibited reduced degradation efficiencies of 40.7%, and 31.8%, respectively, as shown in Figure 4c. This decline in catalytic performance under alkaline conditions is primarily attributed to the high concentration of hydroxyl ions, which can inhibit oxidation reactions and weaken interactions between dye molecules and the catalyst surface.[51]

In addition to pH-dependent behavior, the role of reaction time in the catalytic degradation of methylene blue (MB) was systematically examined, as illustrated in Figure 7(a). A continuous decrease in MB absorbance was observed with increasing reaction duration, indicating progressive dye degradation. The reaction reached an equilibrium state after approximately 30 min, beyond which no significant change in absorbance was detected. These results demonstrate that degradation efficiency is closely linked to the initial concentration of the dye. To further validate this observation, experiments were conducted using a constant amount of nanocatalyst while varying the initial MB concentration, confirming that both contact time and dye concentration play critical roles in governing catalytic performance.

## 4. CONCLUSIONS

In the present work, pristine and graphene oxide (GO)-modified $MnO_2$ nanorods were successfully synthesized using a facile chemical precipitation approach to investigate the influence of GO incorporation on the catalytic and antibacterial performance of $MnO_2$. Comprehensive characterization was carried out to analyze the structural, optical, morphological, and compositional features of both undoped and GO-doped $MnO_2$ nanorods. X-ray diffraction (XRD) and energy-dispersive spectroscopy (EDS) analyses confirmed the formation of phase-pure monoclinic $MnO_2$ with an average crystallite size of approximately 36.4 nm, along with the effective incorporation of GO within the $MnO_2$ matrix. The calculated interplanar spacing and crystallographic plane orientations obtained from XRD were found to be in close agreement with high-resolution transmission electron microscopy (HR-TEM) observations, validating the crystalline nature and nanorod morphology of the synthesized materials.

Optical studies revealed that the UV–visible absorption spectra exhibited a prominent absorption peak around 300 nm corresponding to a band gap energy of approximately 4.1 eV. A noticeable blue shift in the absorption edge was observed upon GO doping, which can be attributed to quantum confinement effects and electronic interactions between GO and $MnO_2$. The photoluminescence emission behavior further indicated the presence of defect states, particularly oxygen vacancies, which are known to play a significant role in enhancing catalytic activity.

Catalytic performance evaluated through methylene blue degradation under dark conditions demonstrated a remarkable enhancement in activity for GO-doped $MnO_2$ nanorods. The sample containing 6% GO exhibited up to 94% degradation efficiency in acidic medium and approximately 95% degradation in neutral medium, highlighting the crucial role of GO in facilitating charge transfer and increasing the availability of active catalytic sites.

## REFERENCES


1. Tayyebi, A., Outokesh, M., Tayebi, M., Shafikhani, A., & Şengör, S. S. (2016). ZnO quantum dots–graphene composites: Formation mechanism and enhanced photocatalytic activity for degradation of methyl orange dye. Journal of Alloys and Compounds, 663, 738–749.
2. Singh, S., Kumar, V., Romero, R., Sharma, K., & Singh, J. (2019). Applications of nanoparticles in wastewater treatment. In Nanobiotechnology in bioformulations (pp. 395–418). Springer.
3. El-Mekkawi, D. M., Abdelwahab, N. A., Mohamed, W. A. A., Taha, N. A., & Abdel-Mottaleb, M. S. A. (2020). Solar photocatalytic treatment of industrial wastewater utilizing recycled polymeric disposals as $TiO_2$ supports. Journal of Cleaner Production, 249, 119430.
4. El-Sayed, B. A., Mohamed, W. A. A., Galal, H. R., Abd El-Bary, H. M., & Ahmed, M. A. M. (2019). Photocatalytic study of synthesized MWCNTs/$TiO_2$ nanocomposites. Egyptian Journal of Petroleum, 28, 247–252.
5. Zeid, E. F. A., Ibrahem, I. A., Ali, A. M., & Mohamed, W. A. A. (2019). Effect of CdO content on NiO/CdO nanocomposite properties. Results in Physics, 12, 562–570.
6. Vaez, Z., & Javanbakht, V. (2020). Photocatalytic activity of ZSM-5/ZnO nanocomposite modified by Ag nanoparticles. Journal of Photochemistry and Photobiology A: Chemistry, 388, 112064.
7. Shashi Shekhar, T. R., Kiran, B. R., Puttaiah, E. T., Shivaraj, Y., & Mahadevan, K. M. (2008). Phytoplankton as an index of water quality. Journal of Environmental Biology, 29, 233.

8. Salem, I. A. (2000). Color removal of Congo red using zirconium oxide catalyst. Transition Metal Chemistry, 25, 599–604.
9. Siddiqui, S. I., Manzoor, O., Mohsin, M., & Chaudhry, S. A. (2019). $MnO_2$/BC nanocomposite for dye degradation and antibacterial activity. Environmental Research, 171, 328–340.
10. Lu, W., Li, J., Sheng, Y., Zhang, X., You, J., & Chen, L. (2017). Magnetic iron oxide–MWCNT composites for Cr(VI) removal. Journal of Colloid and Interface Science, 505, 1134–1146.
11. Varjani, S. J., & Sudha, M. C. (2018). Treatment technologies for emerging contaminants. In Water remediation (pp. 91–115). Springer.
12. Zhu, S., & Wang, D. (2017). Photocatalysis: Principles and applications. Advanced Energy Materials, 7, 1700841.
13. Zhao, L., Deng, J., Sun, P., Liu, J., Ji, Y., Tanaka, H., & Yang, Y. (2018). Nanomaterials for water treatment. Science of the Total Environment, 627, 1253–1263.
14. Tara, N., Siddiqui, S. I., Bach, Q. V., & Chaudhry, S. A. (2018). RGO–$MnO_2$ hybrid composite for photocatalysis. ACS Sustainable Chemistry & Engineering, 6, 965–973.
15. Nanda, B., Pradhan, A. C., & Parida, K. M. (2016). $MnO_2$-modified MCM-41 for dye degradation. Microporous and Mesoporous Materials, 226, 229–242.
16. Yin, B., Zhang, S., Jiao, Y., Liu, Y., Qu, F., & Wu, X. (2014). Ultralong $MnO_2$ nanowires with enhanced photocatalytic activity. CrystEngComm, 16, 9999–10005.
17. Yu, W., Liu, T., Cao, S., Wang, C., & Chen, C. (2016). $MnO_2$/ZnO nanorod hybrids with antibacterial activity. Journal of Solid State Chemistry, 239, 131–138.
18. Xia, P., Zhu, B., Cheng, B., Yu, J., & Xu, J. (2018). g-$C_3N_4$/$MnO_2$ Z-scheme photocatalyst. Chemistry of Materials, 22, 5306–5313.
19. Xiao, Y., Huo, W., Yin, S., Jiang, D., Zhang, Y., Dong, F., & Li, G. (2019). Cu-doped $MnO_2$ for methylene blue degradation. Journal of Colloid and Interface Science, 556, 466–475.
20. Pan, X., Cheng, S., Su, T., Zuo, G., Zhao, W., & Dong, W. (2019). $Fe_3O_4$@$MnO_2$ catalyst for wastewater treatment. Colloids and Surfaces B, 181, 226–233.
21. Mittal, N., Shah, A., Punjabi, P. B., & Sharma, V. K. (2009). Photodegradation of Rose Bengal using $MnO_2$. Rasayan Journal of Chemistry, 2, 516–520.
22. Su, P., Chu, D., & Wang, L. (2010). Catalytic activity of $Mn_2O_3$ nanostructures. Modern Applied Science, 4, 125–129.
23. Kang, M., Park, E. D., Kim, J. M., & Yie, J. E. (2007). Manganese oxide catalysts for NOx reduction. Applied Catalysis A, 327, 261–269.
24. Chu, X., & Zhang, H. (2009). Catalytic decomposition of formaldehyde on $MnO_2$. Modern Applied Science, 3, 177–181.
25. Zhang, G., Yang, J., Zhang, S., Xiong, Q., & Huang, B. (2009). Nanosized $Bi_3NbO_7$ photocatalyst. Journal of Hazardous Materials, 172, 986–992.
26. Haile, H. L., Abi, T., & Tesfahun, K. (2015). $MnO_2$/$Al_2O_3$/$Fe_2O_3$ nanocomposite for dye degradation. African Journal of Pure and Applied Chemistry, 9, 211–222.
27. Zhang, J., Wang, L., Wu, Z., Wang, H., & Xiao, F.-S. (2020). Mesoporous Co-Al oxide nanosheets. AIChE Journal, 66, e16923.
28. Mahlangeni, N. T., Magura, J., Moodley, R., Baijnath, H., & Chenia, H. (2020). Antimicrobial activity of $MnO_2$ nanoparticles. Chemical Papers, 74, 4253–4265.
29. Cruz, M., Gomez, C., Duran-Valle, C. J., & Bahamonde, A. (2017). $TiO_2$ and GO photocatalysts for pesticide degradation. Applied Surface Science, 416, 1013–1021.
30. Jiang, X., Nisar, J., Pathak, B., Zhao, J., & Ahuja, R. (2013). Graphene oxide as visible-light photocatalyst. Journal of Catalysis, 299, 204–209.
31. Wang, D., Choi, D., Li, J., Yang, Z., & Liu, J. (2009). $TiO_2$–graphene hybrid nanostructures. ACS Nano, 3, 907–914.
32. Ning, F., Peng, H., Li, J., Chen, L., & Xiong, H. (2014). Magnetic graphene oxide for estradiol extraction. Journal of Agricultural and Food Chemistry, 62, 7436–7443.
33. Zhou, G., Wang, D. W., Li, F., Zhang, L., & Cheng, H. M. (2010). Graphene-wrapped FeO anode materials. Chemistry of Materials, 22, 5306–5313.
34. Zhu, Y., Murali, S., Cai, W., Li, X., Suk, J. W., & Ruoff, R. S. (2010). Graphene and graphene oxide. Advanced Materials, 22, 3906–3924.
35. Santhosh, K. K., Modak, M. D., & Paik, P. (2017). Graphene oxide for biomedical applications. Journal of Nanomedicine Research, 5, 00136.
36. Sachdeva, H. (2020). Catalytic applications of GO/RGO. Green Processing and Synthesis, 9, 515–537.
37. He, Q., Liu, J., Liu, X., Li, G., Chen, D., & Liang, J. (2019). $MnO_2$ nanowires/graphene composites for dopamine sensing. Electrochimica Acta, 296, 683–692.

38. He, Q., Liu, J., Liu, X., Li, G., Deng, P., & Liang, J. (2018). $MnO_2$ nanorods/graphene electrodes for dye detection. Colloids and Surfaces B, 172, 565–572.
39. Liu, H., Lv, T., Wu, X., Zhu, C., & Zhu, Z. (2014). CdS@RGO microspheres. Applied Surface Science, 305, 242–246.
40. Kumara, B. M. P., Karikkat, S., Krishna, S. H., & Nagabhushana, B. M. (2014). Nano-$MnO_2$ for dye adsorption. Research and Reviews: Journal of Material Sciences, 2, 27–31.
41. Mu, B., Zhang, W., Shao, S., & Wang, A. (2014). Graphene–$MnO_2$–polyaniline composites. Physical Chemistry Chemical Physics, 16, 7872–7880.
42. Wang, H., Lu, Z., Qian, D., Li, Y., & Zhang, W. (2007). α-$MnO_2$ nanorods. Nanotechnology, 18, 115616.
43. Toufiq, A. M., Wang, F., & Javed, Q. U. A. (2013). $MnO_2$ nanostructures by hydrothermal route. Journal of Nanoscience and Nanotechnology, 13, 2948–2952.
44. Paredes, J. I., Villar-Rodil, S., Martínez-Alonso, A., & Tascón, J. M. D. (2008). Graphene oxide dispersions. Langmuir, 24, 10560–10564.
45. Senthil Kumar, P., Selvakumar, M., Babu, S. G., & Chattopadhyay, S. (2015). CuO/chitosan nanocomposite thin film. RSC Advances, 5, 57493–57501.
46. Pai, Y. H., & Tsai, C. T. (2013). β-$MnO_2$-based photoelectrochemical cell. International Journal of Hydrogen Energy, 38, 4342–4350.
47. Song, L., Zhang, S., Wu, X., & Wei, Q. (2012). $Mn(IO_3)_2/MnO_2$ nanostructures. Chemical Engineering Journal, 187, 385–390.
48. Cuong, T. V., Pham, V. H., Tran, Q. T., & Kim, E. J. (2010). Raman studies of graphene films. Materials Letters, 64, 399–401.
49. Goumri, M., Venturini, J. W., Bakour, A., & Baitoul, M. (2016). Optical properties of functionalized graphene oxide. Applied Physics A, 122, 212.
50. Ikram, M., Hayat, S., Imran, M., Haider, A., Naz, S., & Nabgan, W. (2021). Ag/cellulose-doped $CeO_2$ quantum dots. Carbohydrate Polymers, 269, 118346.
51. Ikram, M., Inayat, T., Haider, A., Ul-Hamid, J., & Saeed, A. (2021). GO-doped MgO nanostructures. Nanoscale Research Letters, 16, 56.